Skewed quark distribution of the pion in the light-front quark model

Ho-Meoyng Choi[a], Chueng-Ryong Ji[b] and L.S. Kisslinger[a]
[a] Department of Physics, Carnegie-Mellon University
Pittsburgh, PA 15213
[b]Department of Physics, North Carolina State University
Raleigh, NC 27695-8202

We calculate the skewed quark distributions(SQDs) of the pion in the light-front quark model, and discuss the calculation of the nonvalence contribution to the SQDs in this model. The frame-independence of our model calculation is guaranteed by the constraint of the sum rule between the SQDs and form factor. Our numerical results show large nonvalence contributions to the SQDs at small momentum transfer region as the skewedness increases.

PACS number(s): 13.40.Gp, 13.60.Fz, 12.39.Ki

I. INTRODUCTION

Recently there has been a great interest in the off-forward (or nonforward, off-diagonal) parton distribution functions defined as non-diagonal hadronic matrix elements of bi-local products of the light-front quark and gluon field operators [1,2,3,4,5,6,7,8,9,10]. The off-forward parton distribution functions, the so called "skewed parton distributions (SPDs)", are the generalization of the ordinary (forward) distribution functions. A well-known and practical example of SPDs as a nonperturbative information entering the light-front dominated hard scattering processes is the deeply virtual Compton scattering (DVCS) $\gamma^* p \to \gamma p$ for large initial photon virtuality Q^2 and small t region, which can be factorized into a hard photon-parton and a skewed parton distribution [1,2,3].

In the present work we formulate the pion form factor in terms of the SPDs. Since the usual local photon vertex in the pion form factor analysis is replaced by a nonlocal operator of the SPDs, one can explore new physics. The physical interpretation of the SPDs becomes clear in the light-front frame with the light-front gauge $A^+ = 0$. In the light-front coordinates, the SPDs are in general functions of the longitudinal momentum fraction variable x, the skewedness parameter $\xi = (P - P')^+/P^+$ measuring asymmetry between initial (P) and final (P') hadron state momenta, and the squared momentum transfer t. A simple physical interpretation of the SPDs, in light-front quantization, is that they provide a link between the ordinary parton distributions of hadrons and the hadronic form factors, i.e. the ordinary parton distributions are forward ($\xi = 0$ and $t = 0$) limits of the SPDs and the form factors are given by moments of them.

Due to this dual role of SPDs, they are closely related to form factors with the only difference between SPDs and form factors being that the momentum of the "probed quark" in SPDs is not integrated over but rather kept fixed at momentum fraction x. For example, in studying the light-front wave functions of hadrons, the overlap representation of the light-front wave functions of hadrons for the form factors in spacelike ($q^2 < 0$) region can be obtained if one uses $J^+(= J^0 + J^3)$ and the Drell-Yan-West ($q^+ = 0$) frame where only parton-number-conserving valence Fock state contribution is needed. The successful phenomenological calculations of form factors in spacelike region can be found in the light-front quark model(LFQM) [11,12,13,14]. On the other hand, form factors in timelike ($q^2 > 0$) region such as the weak form factors for exclusive semileptonic decays require $q^+ > 0$ frame, which in turn require parton-number-changing nonvalence Fock state contribution as well as the valence one [15,16]. Similarly, while the ordinary parton distributions (analogous to $q^+ = 0$ limit of form factor) can be represented in terms of squared light-front wave function of a hadron, one cannot avoid nonvalence contributions to SPDs since they always involve non-zero ξ corresponding to $q^+ \neq 0$ in timelike form factor calculations. In recent papers [8,10], the nonvalence contribution to the SPDs has been rewritten in terms of light-front wave functions with different parton configurations. However, the representation given by [8,10] requires to find all the higher Fock-state wave functions while there has been relatively little progress in computing the basic wave functions of hadrons from first principles. Our approach provides an alternative way of handling the nonvalence contribution which is more suitable for the constituent quark model(CQM) specific to the low momentum transfer processes. We use the light-front Bethe-Salpeter (B-S) formalism for the SPDs as an extension of our treatment of the pion form factor [14]. Although the present work has many features similar to that of the Fock state expansion, we utilize the close relation in the B-S formalism between what is interpreted as the valence and nonvalence wave functions in the Fock state approach.

In an effort to apply light-front wave function based phenomenology to form factors in timelike exclusive processes, we have presented in [16] an effective treatment of handling the nonvalence contribution to the weak form factors, based on the B-S formalism, and obtained reasonably good numerical results for the processes in the small momentum transfer region. The main purpose of the present work is to apply the effective method presented in [16] of handling the nonvalenece contribution

to the SPDs of pion at small momentum transfer region in LFQM. The paper is organized as follows. In Section II, we briefly introduce the necessary kinematics in which we follow the notation employed by Radyushkin [3]. In Section III, we represent the SPDs of the pion in terms of light-front vertex functions, starting from the covariant Bethe-Salpeter model of $(3+1)$-dimensional fermion field theory. The nonvalence part of SPDs is expressed in terms of light-front vertex functions of a hadron and a gauge boson. The link operator connecting $(n-1)$-body to $(n+1)$-body in a Fock state representation is obtained by an analytic continuation of the usual B-S amplitude. We also show that the complicated $(n+2)$-body energy denominators are absent through the calculation of the light-front time-ordered diagrams. Of particular interest, the instantaneous contribution of the quark propagator to the nonvalence diagram is seperated from the on-shell propagating part. In Section IV, we replace the light-front vertex functions obtained from Sec. III with our LFQM wave function [12] and show our numerical results for the SPDs of the pion at small momentum transfer region. We also show that the frame-independence of our model is guaranteed by the sum rule between the SPDs and form factor of the pion. Conclusions follow in Section V.

II. KINEMATICS

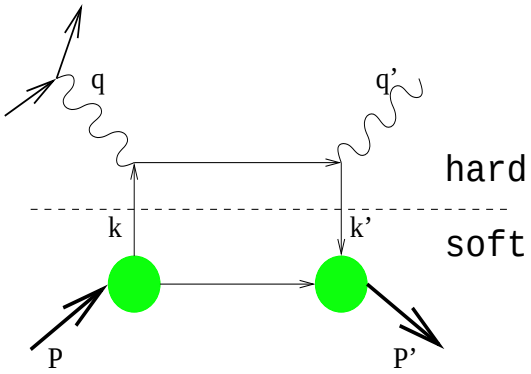

FIG. 1. Handbag diagram contributing dominantly to Compton scattering in the deeply virtual region. The lower soft part consists of a hadronic matrix element which is parametrized in the form of skewed parton distribution functions.

We begin with the kinematics of the virtual Compton scattering (see Fig. 1) of the pion

$$\gamma^*(q) + \pi(P) \to \gamma(q') + \pi(P'), \tag{1}$$

where the initial (final) hadron state is characterized by the momentum P (P') and the incoming spacelike virtual and outgoing real photon momenta by q and q', respectively. We shall use the component notation $V = (V^+, V^-, \mathbf{V}_\perp)$ and our metric is specified by $V^\pm = (V^0 \pm V^3)$ and $V^2 = V^+V^- - \mathbf{V}_\perp$.

Defining the four momentum transfer $\Delta = P - P'$, one has

$$P = \left[P^+, \frac{M^2}{P^+}, 0_\perp\right],$$
$$P' = \left[(1-\xi)P^+, \frac{M^2+\Delta_\perp^2}{(1-\xi)P^+}, -\Delta_\perp\right], \tag{2}$$

and

$$\Delta = P - P' = \left[\xi P^+, \frac{\Delta^2+\Delta_\perp^2}{\xi P^+}, \Delta_\perp\right], \tag{3}$$

where M is the pion mass and $\xi = \Delta^+/P^+$ is the skewedness parameter describing the asymmetry in plus momentum. The squared momentum transfer then reads

$$t = \Delta^2 = 2P\cdot\Delta = -\frac{\xi^2 M^2 + \Delta_\perp^2}{1-\xi}. \tag{4}$$

Since $\Delta_\perp^2 \geq 0$, t has a minimum value $-t_{\rm min} = \xi^2 M^2/(1-\xi)$ at given ξ. As shown in Fig. 1, the parton emitted by the pion has the momentum k, and the one absorbed has the momentum k'.

As in the case of spacelike form factors, we choose a frame where the incident spacelike photon carries $q^+ = 0$:

$$q = \left[0, \frac{(\mathbf{q}_\perp+\Delta_\perp)^2}{\xi P^+} + \frac{\xi M^2+\Delta_\perp^2}{(1-\xi)P^+}, \mathbf{q}_\perp\right],$$
$$q' = \left[\xi P^+, \frac{(\mathbf{q}_\perp+\Delta_\perp)^2}{\xi P^+}, \mathbf{q}_\perp+\Delta_\perp\right]. \tag{5}$$

In deeply virtual Compton scattering (DVCS) where $Q^2 = -q^2$ is large compared to the mass M and $-t$, one obtains

$$\frac{Q^2}{2P\cdot q} = \xi, \tag{6}$$

i.e. ξ plays the role of the Bjorken variable in DVCS. For a fixed value of $-t$, the allowed range of ξ is given by

$$0 \leq \xi \leq \frac{(-t)}{2M^2}\left(\sqrt{1+\frac{4M^2}{(-t)}} - 1\right). \tag{7}$$

III. SKEWED QUARK DISTRIBUTION OF THE PION

Analogous to the pion electromagnetic (EM) form factor calculation

$$J^+(0) \equiv \langle P'|\bar\psi(0)\gamma^+\psi(0)|P\rangle = F_\pi(t)(P+P')^+, \tag{8}$$

we define the skewed quark distributions(SQDs) $\mathcal{F}_\pi(\xi, x, t)$ of a pion by

$$\mathcal{J}^+ \equiv \int \frac{dz^-}{4\pi} e^{ixP^+z^-/2} \langle P'|\bar{\psi}(0)\gamma^+\psi(z)|P\rangle|_{z^+=\mathbf{z}_\perp=0}$$
$$= \mathcal{F}_\pi(\xi,x,t)(P+P')^+, \tag{9}$$

where $z = (z^+, z^-, \mathbf{z}_\perp)$ in a light-front representation. Note that the path-ordered exponential of the gauge field, $\mathcal{P}\exp[i\int z^\mu A_\mu]$, required by gauge invariance in Eq. (9) does not appear in the light-front gauge $A^+ = 0$. As one can see from Eqs. (8) and (9), the $\mathcal{F}_\pi$ involves one less integration than the form factor F_π due to nonlocality of the current matrix element. The SQDs display characteristics of the ordinary(forward) quark distribution in the limit of $\xi \to 0$ and $t \to 0$, on the other hand, the first moment of the SQDs is related to the form factor by the following sum rules [2,3]:

$$\int_0^1 dx\ \mathcal{F}_\pi(\xi,x,t) = F_\pi(t), \tag{10}$$

where $\mathcal{F}_\pi(\xi,x,t) = e_u\mathcal{F}_\pi^u(\xi,x,t) - e_d\mathcal{F}_\pi^{\bar{d}}(\xi,x,t)$ and we assume isospin symmetry($m_u = m_{\bar{d}}$) so that $\mathcal{F}_\pi^u(\xi,x,t) = \mathcal{F}_\pi^{\bar{d}}(\xi,x,t)$. Note that Eq. (10) is independent of ξ, which provides important constraints on any model calculation of the SQDs. In general, the polynomiality conditions for the moments of the SQDs [20,21] defined by

$$\int_0^1 dx\ x^{n-1}\mathcal{F}(\xi,x,t) = F_n(\xi,t), \tag{11}$$

require that the highest power of ξ in the polynomial expression of $F_n(\xi,t)$ should not be larger than n. These polynomiality conditions are fundamental properties of the SQDs which follow from the Lorentz invariance. In case of a spin-1/2 composite system [2,8], where the helicity non-flip(H) and helicity flip(E) SQDs are involved, the second($n = 2$) moment of each SQD yields the ξ dependent form factors of the energy-momentum tensor, although the sum of the moments produces the ξ-independent form factors of the energy-momentum tensor. When the sum rule($n = 2$) is extrapolated to $-t = 0$ [2], it provides the information on the total quark(i.e. quark orbital) contribution to the nucleon spin. For the spin-0 composite system like the pion, the situation is quite different because only one SQD $\mathcal{F}(\xi,x,t)$ exists. We discuss our numerical results of $F_n(\xi,t)(n = 1,2,3)$ for the pion in the next section (Section IV).

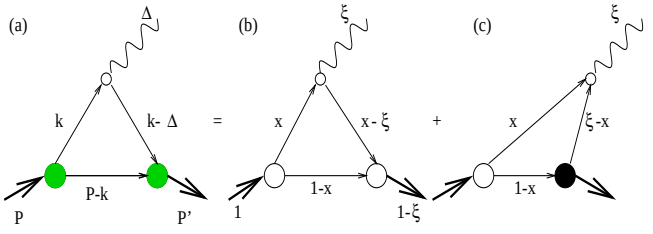

FIG. 2. Diagrams for SQDs in different kinematic regions for the case $\xi > 0$: The covariant diagram (a) corresponds to the sum of the LF valence diagram (b) defined in $\xi < x < 1$ region and the nonvalence diagram (c) defined in $0 < x < \xi$ region. The large white and black blobs at the meson-quark vertices in (b) and (c) represent the ordinary LF wave function and the nonvalence wave function vertices, respectively. The small white blob at the quark-gauge boson vertex indicates the nonlocality of the vertex.

In Refs. [8,10], the overlap representation of light-front wave function for the SQDs has been obtained from the formal definitions of light-front field operators. In this work, however, we shall derive the SQDs of the pion starting from the covariant Bethe-Salpeter (B-S) amplitude of the current $\mathcal{J}$ given by (see Fig. 2(a))

$$\mathcal{J}^\mu = iN_c \int \frac{d^4k}{(2\pi)^4} \frac{\delta(x-k^+/P^+)H_{\rm cov}H'_{\rm cov}S^\mu}{[k^2-m^2+i\epsilon][(k-\Delta)^2-m^2+i\epsilon]}$$
$$\times \frac{1}{[(P-k)^2-m^2+i\epsilon]}, \tag{12}$$

where N_c is the color factor, $\delta(x-k^+/P^+)$ represents the composite operator [3] denoted by a small white blob at the quark-gauge boson vertex in Fig. 2, and $H_{\rm cov}$ ($H'_{\rm cov}$) is the covariant initial (final) state meson-quark vertex function that satisfies the B-S equation. We refer to the black vertex in Fig. 2(c) as the nonvalence wave function vertex as in the B-S formalism it is obtained by a continuation of the usual B-S amplitude, as we discuss below.

Using the following identity

$$\not{p} + m = (\not{p}_{\rm on} + m) + \frac{1}{2}\gamma^+(p^- - p^-_{\rm on}), \tag{13}$$

we can express the trace term S^μ in Eq. (12) in terms of the on-mass shell propagating part of quark propagators and the instantaneous one as follows

$$S^\mu = {\rm Tr}\Big[\gamma_5(\not{p}_1+m)\gamma^\mu(\not{p}_2+m)\gamma_5(-\not{p}_{\bar{q}}+m)\Big]$$
$$= {\rm Tr}\Big[\gamma_5(\not{p}_{1{\rm on}}+m)\gamma^\mu(\not{p}_{2{\rm on}}+m)\gamma_5(-\not{p}_{\bar{q}{\rm on}}+m)\Big]$$
$$+ {\rm Tr}\Big[{\rm inst.}\Big], \tag{14}$$

with

$${\rm Tr}\Big[{\rm inst.}\Big] = 2(p_1^- - p_{1{\rm on}}^-)\Big[p^\mu_{2{\rm on}}p^+_{\bar{q}{\rm on}} - p^+_{2{\rm on}}p^\mu_{\bar{q}{\rm on}}$$
$$+g^{\mu+}(p_{2{\rm on}}\cdot p_{\bar{q}{\rm on}} + m^2)\Big]$$
$$+ 2(p_2^- - p_{2{\rm on}}^-)\Big[p^\mu_{1{\rm on}}p^+_{\bar{q}{\rm on}} - p^+_{1{\rm on}}p^\mu_{\bar{q}{\rm on}}$$
$$+g^{\mu+}(p_{1{\rm on}}\cdot p_{\bar{q}{\rm on}} + m^2)\Big]$$

$$+ 2(p_{\bar{q}}^- - p_{\bar{q}\rm on}^-)\Big[p_{1\rm on}^\mu p_{2\rm on}^+ + p_{1\rm on}^+ p_{2\rm on}^\mu - g^{\mu+}(p_{1\rm on}\cdot p_{2\rm on} + m^2)\Big] + 2g^{\mu+}p_{\bar{q}\rm on}^+(p_1^- - p_{1\rm on}^-)(p_2^- - p_{2\rm on}^-), \quad (15)$$

where $p_1 = k, p_2 = k - \Delta$, and $p_{\bar{q}} = P - k$ and the subscript (on) means on-mass shell quark propagator.

The SQD is given by the solutions to the B-S equation [16,17,18]

$$(M_\xi^2 - \mathcal{M}_0^2)\chi(x_i, \mathbf{k}_{i\perp}) = \int [dy][d^2\mathbf{l}_\perp]\mathcal{K}(x_i, \mathbf{k}_{i\perp}; y_j, \mathbf{l}_{j\perp})\chi(y_j, \mathbf{l}_{j\perp}), \quad (16)$$

where $\mathcal{K}$ is the B-S kernel which in principle includes all the higher Fock-state contributions, $M_\xi = M^2/(1-\xi)$, $\mathcal{M}_0^2 = (m^2 + \mathbf{k}_\perp^2)/(1-x) - (m^2 + \mathbf{k}_\perp^2)/(\xi - x)$, and $\chi(x_i, \mathbf{k}_{i\perp})$ is the B-S amplitude. Both the valence and nonvalence B-S amplitudes are solutions to Eq. (16). For the normal B-S amplitude, referred to as the valence wave function here, $x > \xi$, while for the nonvalence B-S amplitude $x < \xi$. We use the notation for these two solutions

$$\chi_{(2\to 2)} = \chi^{val}$$
$$\chi_{(1\to 3)} = \chi^{nonval}. \quad (17)$$

This notation is motivated by the relationship to the Fock state picture, in which for the nonvalence vertex the parton number before and after the kernel is interpreted as changing (from 1 to 3). However, as illustrated in Fig. 2(c), the nonvalence B-S amplitude is an analytic continuation of the valence B-S amplitude. In the LFQM the relationship between the B-S amplitudes in the two regions is given by [16]

$$(M_\xi^2 - \mathcal{M}_0^2)\chi_{(1\to 3)}(x_i, \mathbf{k}_{i\perp}) = \int [dy][d^2\mathbf{l}_\perp]\mathcal{K}(x_i, \mathbf{k}_{i\perp}; y_j, \mathbf{l}_{j\perp})\chi_{(2\to 2)}(y_j, \mathbf{l}_{j\perp}), \quad (18)$$

where again the kernel includes in principle all the higher Fock-state contributions because all the higher Fock components of the bound-state are ultimately related to the lowest Fock component with the use of kernel. This is illustrated in Fig. 3.

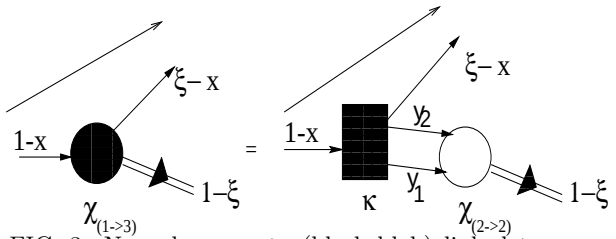

FIG. 3. Nonvalence vertex(black blob) linked to an ordinary light-front wave function(white blob).

Equations (16) and (18) are integral equations for which one needs nonperturbative QCD to obtain the kernel. We do not solve for the B-S amplitudes in this work, but a nice feature of Eq. (18) is a natural link between χ^{nonval} and χ^{val} which enables an application of a light-front CQM even for the calculation of nonvalence contribution in Fig. 2(c). We describe this below. In 1 + 1 QCD models [9,19], it is shown that expressions for the nonvalence vertex analogous to our form given in Eq.(18) are obtained.

Corresponding to these two regions of the B-S amplitude, the Cauchy integration over k^- in Eq. (12) has two nonzero contribution to the residue calculations, one coming from the interval (I) $\Delta^+ < k^+ < P^+$ [see Fig. 2(b)] and the other from (II) $0 < k^+ < \Delta^+$ [see Fig. 2(c)].

(I) In the region of $\Delta^+ < k^+ < P^+$, the residue is at the pole of $k^- = P^- - [\mathbf{k}_\perp^2 + m^2 - i\epsilon]/(P-k)^+$(i.e. $p_{\bar{q}}^- = p_{\bar{q}\rm on}^-$), which is placed in the upper half of complex-k^- plane. Thus, the Cauchy integration of $\mathcal{J}^+$ in Eq. (12) over k^- gives

$$\mathcal{F}_\pi^{val}(\xi, x, t) = \frac{N_c}{(P+P')^+}\int_\xi^1 \frac{dx}{16\pi^3}\frac{\delta(x - k^+/P^+)}{x(1-x)x'} \times \int d^2\mathbf{k}_\perp \chi_{(2\to 2)}(x, \mathbf{k}_\perp) S_{val}^+ \chi'_{(2\to 2)}(x', \mathbf{k}'_\perp), \quad (19)$$

where

$$\chi_{(2\to 2)} = \frac{h_{LF}}{M^2 - M_0^2}, M_0^2 = \frac{\mathbf{k}_\perp^2 + m^2}{1-x} + \frac{\mathbf{k}_\perp^2 + m^2}{x},$$
$$\chi'_{(2\to 2)} = \frac{h'_{LF}}{M^2 - M_0'^2}, M_0'^2 = \frac{\mathbf{k}'^2_\perp + m^2}{1-x'} + \frac{\mathbf{k}'^2_\perp + m^2}{x'}, \quad (20)$$

and

$$S_{val}^+ = \frac{4P^+}{(1-x')}(\mathbf{k}_\perp \cdot \mathbf{k}'_\perp + m^2). \quad (21)$$

The internal momenta of the (struck) quark for the final state are given by

$$x' = \frac{x-\xi}{1-\xi}, \quad \mathbf{k}'_\perp = \mathbf{k}_\perp + \frac{1-x}{1-\xi}\Delta_\perp. \quad (22)$$

While the light-front vertex function h_{LF} (h'_{LF}) formally is given by the covariant $H_{\rm cov}$ ($H'_{\rm cov}$), in the present work the radial wave function $\chi_{(2\to 2)}$ ($\chi'_{(2\to 2)}$) [consequently h_{LF} (h'_{LF})] is obtained from a light-front constituent quark model as we shall show later. It is also interesting to note that in this spectator pole diagram ($p_{\bar{q}}^- = p_{\bar{q}\rm on}^-$) with the plus component of the current, the instantaneous part in Eq. (15) does not contribute at all, i.e. all particles are on their mass shell.

(II) In the region of $0 < k^+ < \Delta^+$, the residue is at the pole of $k^- = [\mathbf{k}_\perp^2 + m^2 - i\epsilon]/k^+$ (i.e. $p_1^- = p_{1\rm on}^-$), which is

placed in the lower half of complex-k^- plane. Then the Cauchy integration of $\mathcal{J}^+$ in Eq. (12) over k^- reads

$$\begin{aligned}
&\mathcal{F}_\pi^{nv}(\xi,x,t)\\
&=\frac{N_c}{(P+P')^+}\int_0^\xi \frac{dx}{16\pi^3}\frac{\delta(x-k^+/P^+)}{x(1-x)x'}\\
&\times\int d^2\mathbf{k}_\perp \chi_{(2\to 2)}(x,\mathbf{k}_\perp)S^+_{nv}\chi^g(x,\mathbf{k''}_\perp)\\
&\times\int\frac{dy}{y(1-y)}\int d^2\mathbf{l}_\perp \mathcal{K}(x,\mathbf{k}_\perp;y,\mathbf{l}_\perp)\chi_{(2\to 2)}(y,\mathbf{l}_\perp),
\end{aligned} \tag{23}$$

where Eq. (18) has been used for the nonvalence wave function at the black blob in Fig. 2(c), and χ^g corresponds to the light-front energy denominator at the small white blob in Fig. 2(c). The explicit form of χ^g is given by

$$\chi^g(x,\mathbf{k''}_\perp)=\frac{1}{(1-\xi)\left[\frac{\Delta^2}{\xi}-\left(\frac{\mathbf{k''}_\perp^2+m^2}{x}+\frac{\mathbf{k''}_\perp^2+m^2}{\xi-x}\right)\right]}, \tag{24}$$

where $\mathbf{k''}_\perp=\mathbf{k}_\perp+(x/\xi)\Delta_\perp$. We call χ^g the light-front vertex function of a gauge boson [1]. In the calculation of the trace term S^+_{nv}, one can easily see from Eq. (15) that there is one instantaneous contribution from the spectator ($p_{\bar q}$) line in addition to the on-mass shell contribution given by Eq. (21), which leads to

$$S^+_{nv}=S^+_{val}+\frac{4P^+}{1-x'}x(1-x)x'(M^2-M_0^2). \tag{25}$$

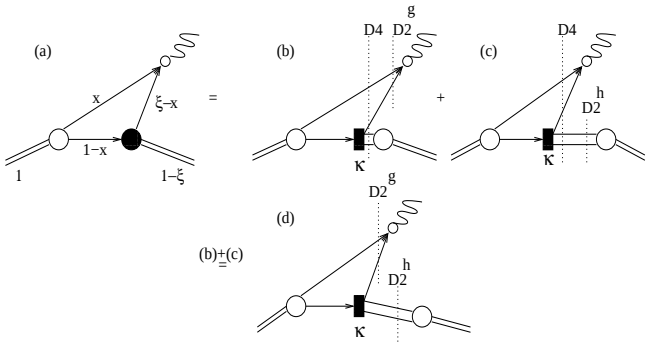

FIG. 4. Effective treatment of the light-front nonvalence amplitude given by Fig. 2(c).

[1] While one can in principle also consider the B-S amplitude for χ^g, we note that such extension does not alter our results within our approximation in this work because both hadron and gauge boson should share the same kernel.

Considering the quark-meson and quark-gauge boson vertices together, we also find that the four-body energy denominator (D_4) appearing in Fig. 3 is absent in Eq. (23). This absence of D_4 in our nonvalence current matrix amplitude given by Eq. (23) is due to the sum of two possible diagrams in the light-front time-ordering (see Figs. 4(b) and (c)). Summing over the two time-ordered diagrams Figs. 4(b) and (c), one can easily find the following identity, $1/D_4D_2^g+1/D_4D_2^h=1/D_2^gD_2^h$, which removes the complicate four-body energy denominator term. We thus obtain the amplitude corresponding to the nonvalence contribution given by Eq. (23) in terms of ordinary light-front wave functions of hadron ($\chi_{(2\to 2)}$) and gauge boson (χ^g) as shown in Fig. 4(d). This method, however, requires the relevant operator $\mathcal{K}(x,\mathbf{k}_\perp;y,\mathbf{l}_\perp)$ which is in general dependent on the involved momenta connecting the one-body to three-body sector as depicted in Fig. 3. While the relevant operator $\mathcal{K}$ is in general dependent on all internal momenta $(x,\mathbf{k}_\perp;y,\mathbf{l}_\perp)$, the integral of $\mathcal{K}$ over y and $\mathbf{l}_\perp$ in Eq. (23), which we define as $G_\pi\equiv\int[dy][d^2\mathbf{l}_\perp]\mathcal{K}(x,\mathbf{k}_\perp;y,\mathbf{l}_\perp)\chi_{(2\to 2)}(y,\mathbf{l}_\perp)$, depends only on x and $\mathbf{k}_\perp$. In this work, we approximate G_π as a constant which has been tested in our previous exclusive semileptonic decay processes [16] and proved to be a good approxiamtion at least for small momentum transfer region. As we shall show in the next section, the validity of this approximation can be checked by examining the frame-independence of our numerical results.

IV. MODEL CALCULATION OF SQD

In the previous sections we have derived the skewed quark distribution function $\mathcal{F}_\pi(\xi,x,t)$ starting from a covariant model. In this section we replace the light-front vertex function h_{LF} (or equivalently $\chi_{(2\to 2)}(x,\mathbf{k}_\perp)$) by the standard light-front vertex function [11,12,13], which is symmetric in the variables of the constituent $q\bar q$ pair and has been successful in predicting many static properties of ground state mesons. Different choices of the vertex function are of course possible.

Comparing $\chi_{(2\to 2)}$ with our light-front wave function given by Ref. [12], we identify

$$\chi_{(2\to 2)}(x,\mathbf{k}_\perp)=\sqrt{\frac{8\pi^3}{N_c}}\sqrt{\frac{\partial k_z}{\partial x}}\frac{[x(1-x)]^{1/2}}{M_0}\phi(x,\mathbf{k}_\perp), \tag{26}$$

where the Jacobian of the variable tranformation $\mathbf{k}=(k_z,\mathbf{k}_\perp)\to(x,\mathbf{k}_\perp)$ is obtained as $\partial k_z/\partial x=M_0/[4x(1-x)]$ and the radial wave function is given by

$$\phi(\mathbf{k}^2)=\sqrt{\frac{1}{\pi^{3/2}\beta^3}}\exp(-\mathbf{k}^2/2\beta^2), \tag{27}$$

which is normalized as $\int d^3k|\phi(\mathbf{k}^2)|^2=1$.

Substituting Eqs. (26) and (27) into Eqs. (19) and (23), we obtain the valence and nonvalence contributions to the SQDs of the pion in LFQM

$$\mathcal{F}_\pi^{val}(\xi,x,t) = \frac{\theta(x-\xi)}{1-\frac{\xi}{2}} \int d^2\mathbf{k}_\perp \sqrt{\frac{\partial k'_z}{\partial x'}}\sqrt{\frac{\partial k_z}{\partial x}}\phi(x',\mathbf{k'}_\perp) \times\phi(x,\mathbf{k}_\perp)\frac{(\mathbf{k}_\perp\cdot\mathbf{k'}_\perp+m^2)}{\sqrt{\mathbf{k}_\perp^2+m^2}\sqrt{\mathbf{k'}_\perp^2+m^2}}, \quad (28)$$

and

$$\mathcal{F}_\pi^{nv}(\xi,x,t) = \frac{\theta(\xi-x)}{1-\frac{\xi}{2}} \int d^2\mathbf{k}_\perp \sqrt{\frac{\partial k_z}{\partial x}}\phi(x,\mathbf{k}_\perp)\chi^g(x,\mathbf{k''}_\perp) \times \frac{\mathbf{k}_\perp\cdot\mathbf{k'}_\perp+m^2+x(1-x)x'(M^2-M_0^2)}{x'(1-x')\sqrt{\mathbf{k}_\perp^2+m^2}} \times \int_0^1 dy \int d^2\mathbf{l}_\perp \sqrt{\frac{\partial l_z}{\partial y}}\frac{\mathcal{K}(x,\mathbf{k}_\perp;y,\mathbf{l}_\perp)}{\sqrt{\mathbf{l}_\perp^2+m^2}}\phi(y,\mathbf{l}_\perp), \quad (29)$$

where we treat the last term in Eq. (29) as a constant G_π which will be fixed by the sum rule expressed in terms of $\mathcal{F}_\pi^{val}$ and $\mathcal{F}_\pi^{nv}$ as

$$F_\pi(t) = \int_\xi^1 dx\ \mathcal{F}_\pi^{val}(\xi,x,t) + \int_0^\xi dx\ \mathcal{F}_\pi^{nv}(\xi,x,t), \quad (30)$$

for given $-t$. We note that Eq. (30) is used as a constraint on the frame-independence of our model.

In our numerical calculations, we use the model parameters $(m,\beta) = (0.22, 0.3659)$ [GeV] obtained in Ref. [12] for the linear confining potential model. Before we calculate the SQDs and the form factor of the pion, we first consider the valence contribution to the pion EM form factor and see how much the nonvalence contribution is needed to obtain the frame-independent result of our model. To this end, we show in Fig. 5 the valence contribution (see Fig. 2(b)) to the pion EM form factor with different values of ξ, where the thick solid, cross (x), dotted, dot-dashed, and thin solid lines represent the purely transverse ($\xi = 0$ and $\Delta_\perp \neq 0$), $\xi = 0.02$, 0.3, 0.6, and the purely longitudinal (i.e. $\xi \neq 0$ and $\Delta_\perp = 0$) results, respectively, and compare with the experimental data [22,23]. Note that the purely transverse frame result (thick solid line) is the exact solution within our model calculation. As one can see from Fig. 5, the nonvalence contribution to the pion form factor, i.e. the difference between $\xi = 0$ and $\xi \neq 0$ results, increases as ξ does. Our special interesting region in this work is the small $-t$ region where the nonvalence contribution is especially large and our effective method for the calculation of the nonvalence contributions works pretty well.

Including the nonvalence contribution given by Eq. (29) to the SQDs of the pion, we can determine our constant G_π in a frame-independent way by the sum rule $\int_0^1 dx\ \mathcal{F}_\pi^{val}(\xi=0,x,t) = \int_\xi^1 dx\ \mathcal{F}_\pi^{val}(\xi\neq 0,x,t) + \int_0^\xi dx\ \mathcal{F}_\pi^{nv}(\xi\neq 0,x,t) = F_\pi(t)$. In Fig. 6, we show the ξ-dependence of G_π for different $-t$-values, i.e. $-t = 0$ (diamond), 0.2 (black circle), 0.5 (white circle), and 1.0 (black square) [GeV^2], respectively. As one can see in Fig. 6, G_π shows approximately constant behavior for $\xi > 0.1$ at given small $-t$. It is not surprising to see that G_π becomes very large as $\xi \to 0$, however, this does not cause a significant error in our calculation because the nonvalence contribution in the very small ξ region is highly suppressed. Note from Eq. (23) that $\mathcal{F}_\pi^{nv}$ has the form of $\mathcal{F}_\pi^{nv} = G_\pi \times \int_0^\xi ...$; thus G_π must be very large as $\xi \to 0$ to give the small contribution of $\mathcal{F}_\pi^{nv}$, since the integral vanishes. Therefore the results are consistent with an almost constant value for G_π at least for small $-t$ as we show below. On the other hand, we note that there is an obvious t-dependence for G_π, which might be the limit of our constant approximation. In principle, we can obtain the SQDs in a frame-independent way by using the true values of G_π as shown in Fig. 6 for given (ξ,t). In the following, we compare the SQDs and the form factor obtained from true values of G_π (i.e. frame-independent result of our model) with those obtained from a single average value of $G_\pi = G_{\rm ave.} = 0.32$ for all (ξ,t) to check the reliability of our constant G_π approximation.

In Figs. 7 and 8, we show the SQDs $\mathcal{F}_\pi(\xi,x,t)$ of the pion for fixed momentum transfer $-t = 0.2$ GeV^2 ($0 \le \xi \le 0.92$) and $-t = 1.0$ GeV^2 ($0 \le \xi \le 0.98$) but with different skewedness parameters ξ, respectively. The solid and cross (x) lines in the nonvalence contributions are the exact solutions obtained from true values of G_π and the effective ones obtained from our average value of $G_{\rm ave.} = 0.32$, respectively. The dotted lines represent the instantaneous contributions to $\mathcal{F}_\pi^{nv}(\xi,x,t)$ obtained from true values of G_π. The SQDs at $\xi = 0$ as shown in Figs. 7(a) and 8(a) correspond to the ordinary quark distributions with vanishing nonvalence contributions. The frame-independence of our model calculation is ensured by the area under the solid lines(valence + nonvalence) being equal to the pion form factor at given $-t$. As one can see from Figs. 7(b-c) and 8(b-c), while the nonvalence contributions are small for small $\xi = 0.3$, they are large for large skewdness parameter $\xi = 0.9$. In our model calculations, the nonvalence contributions obtained from true values of G_π (solid lines in each figure) at $-t$=0.2 (1.0) GeV^2 for ξ=0.3 (0.3) and 0.9 (0.9) are approximately 11 (4) % and 90 (85) %, respectively. Comparing with the exact solutions, the numerical results with a single average $G_{\rm ave.} = 0.32$ (cross lines in each figure) are shown to reproduce the exact ones up to 97 % for $\xi = 0.3$ and 90 % for $\xi = 0.9$, respectively. It is also interesting to note that the instantaneous contribuitons (dotted lines in each figure) become more pronounced as $\xi \to \xi_{\rm max}$ for each $-t$, which is a very different feature from a scalar theory model [9] where there is no such instantaneous contribution. While the instantaneous part of the nonvalence contribution vanishes as $x \to \xi^- = lim_{\epsilon\to 0}(\xi-\epsilon)$ as shown in Figs. 7 and 8, the net

result of $\mathcal{F}_\pi^{nv}(\xi,x,t)$ including the on-mass shell propagating part does not[2] vanish as $x=\xi$ and consequently causes a discontinuity to the zero value of $\mathcal{F}_\pi^{val}(\xi,\xi,t)$. However, such discontinuity at $x=\xi$ is just an artifact due to the difference in the $x\to\xi$ behavior between the gauge boson vertex ($\chi^g(x,\mathbf{k}''_\perp)$) in Eq. (24) and the hadronic vertex ($\chi'_{2\to 2}(x',\mathbf{k}'_\perp)$ in Eq. (19) of our approximate model calculation. We have indeed confirmed that the discontinuity at $x=\xi$ does not occur in the limit of a point hadron vertex as already noticed in the QED calculation [8][3]. Thus, for a full analysis of DVCS satisfying the factorization theorems [24], it would be necessary to solve the bound-state B-S equation similar to Eq. (16) for the gauge boson (χ^g) as well as for the hadron ($\chi_{2\to 2}$). In the chiral quark-soliton model analysis of the nucleon SQDs [24], the discontinuity at $x=\xi$ was imputed to an artifact of neglecting the momentum dependence of the constituent quark mass. Both the B-S amplitude for χ^g and the dynamical quark mass would be anyway necessary for the model improvement. Nevertheless, our effective method seems useful for the present study of the relation between SQDs and the form factor in the nonperturbative regions.

In Fig. 9, we show our effective solutions of the pion form factor for $\xi=0.3$ (thin solid line) and 0.9 (long-dashed line) cases obtained from our average value of $G_\pi=G_{\rm ave.}=0.32$ and compare with the exact solution with $\xi=0$ (thick solid line) as well as the experimental data [22,23]. The dotted and dot-dashed lines represent the valence and the instantaneous contributions to the form factor for the case of $\xi=0.9$, respectively. In fact, there are $-t_{\rm min}$ values for nonzero ξ due to $\Delta_\perp^2\geq 0$ (see Eq. (4)). We thus use the analytic continuation by changing $\Delta_\perp$ to $i\Delta_\perp$ in Eqs. (28) and (29) to obtain the result for $0\leq -t\leq -t_{\rm min}$ where there is no singularity. A continuous behavior of the form factor near $-t_{\rm min}$ confirms the analyticity of our model calculation. Our effective solution (thin solid line) with $\xi=0.9$ shows almost maximum deviation ($\lesssim 10$ %) from the exact one (thick solid line) and the deviation becomes smaller as ξ reduces. Our effective method of evaluating the nonvalence diagram with a constant operator G_π shows a definite improvement to restore the frame-independence of our model and seems to be a quite reliable approximation.

In Fig. 10, we show the nth moments($n=1,2,3$) of $\mathcal{F}_\pi(\xi,x,t)$ given by Eq. (11) at $t=0$ using the true value of G_π shown in Fig. 6. Although at $t=0$ the skewedness parameter vanishes (see Eq. (7)), we use the model forms for $\mathcal{F}_\pi^{val}$ and $\mathcal{F}_\pi^{nv}$ given by Eqs. (28,29) to define the extrapolation to $\xi\neq 0$. The thick solid, dotted, and dot-dashed lines represent the total(=valence + nonvalence), valence, and nonvalence contributions, respectively. For comparison, we also show the nonvalence contribution obtained from the average value of $G_\pi=0.32$(cross lines). As one can see, the first($n=1$) moment (top thick solid line) is ξ-independent because the sum rule for $n=1$ yields the physical pion form factor, $F_1(\xi,t)=F_\pi(t)$. Also, the higher moments $F_2(\xi,t)$(middle thick solid line) and $F_3(\xi,t)$(bottom thick solid line) satisfy the polynomiality conditions(See Eq. (11)) discussed in the previous section. In Fig. 10 we also plot the phenomenological form

$$F_n(\xi,t=0)$$
$$\simeq F_n(\xi=1)-(1-\xi)^2[F_n(\xi=1)-F_n(\xi=0)], \quad (31)$$

shown by the diamonds. The numerical values for $F_n^v=F_n(\xi=0)$ and $F_n^{nv}=F_n(\xi=1)$ are summarized in Table I. Our value of F_3^v is in good agreement with the value obtained by the QCD sum rules with non-local condensates [25].

We also compute the nth moment of the π wave function, $\phi_\pi(y)=\mathcal{F}_\pi(\xi=0,y,t=0)$, defined by [26]

$$\langle y_n\rangle=\int_{-1}^{1}dy y^n\phi_\pi(y) \quad (32)$$

where $y=2x-1$. Our numerical results are summarized in Table II and compared with several other theoretical results. It is interesting to note that our value of $\langle y_2\rangle$ is very close to the asymptotic value (0.2) of the second moment obtained from the well-known asymptotic quark distribution amplitude $\phi_\pi(y)=\frac{3}{4}(1-y^2)$, which is quite different from the early work obtained with QCD sum rules [26] shown in the second row of Table II. A later calculation using QCD sum rules [27], shown in the third row, found moments closer to the asymptotic values. However, we emphasize that the Bethe-Salpeter amplitude used in the present work is a model rather than a solution to the B-S equation with a kernel derived from nonperturbative QCD.

Finally, in Fig.11, we obtain the isosinglet SQDs of the pion by subtracting the valence part $\mathcal{F}_\pi(\xi=0,x,t=0)$ from the nonvalence part $\mathcal{F}_\pi(\xi=1,x,t=0)$. Our result (dotted line) in Fig. 11 is qualitatively very similar to the total isoscalar skewed quark distribution in the pion satisfying the soft pion theorem (Fig. 5 of Ref. [5]), that is obtained by the low-energy effective field theory based on the instanton model of the QCD vacuum.

V. CONCLUSION

In this work, we investigated the SQDs of the pion for small momentum transfer ($-t\leq 1$ GeV^2) region in the light-front quark model. Since the light-front nonvalence contributions to the SQDs of the pion are large especially at small momentum transfer region as shown in Fig. 5, it is very crucial to take them into account to guarantee

[2]In fact, this behavior of $\mathcal{F}_\pi^{nv}(\xi,x,t)$ at $x=\xi$ has been anticipated in [9] without a proof.

[3]We are grateful to M. Diehl for discussion of this point.

the frame-independence of the model. Applying our effective treatment [16], i.e. the nonvalence B-S amplitude given by Eq. (18) of the nonvalence contribution to the SQDs $\mathcal{F}_\pi$ ($=\mathcal{F}_\pi^{val}+\mathcal{F}_\pi^{nv}$) of the pion, we express $\mathcal{F}_\pi^{nv}$ (see Eqs. (23) and (29)) in terms of ordinary light-front wave functions of a gauge boson and a hadron and calculate this nonvalence contribution numerically.

The main approximation in our effective calculation is the treatment of relevant operator $\mathcal{K}(x,\mathbf{k}_\perp;y,\mathbf{l}_\perp)$ in Eq. (23) connecting the one-body to three-body sector (see Fig. 4) by taking a constant G_π via $G_\pi \equiv \int[dy][d^2\mathbf{l}_\perp]\mathcal{K}(x,\mathbf{k}_\perp;y,\mathbf{l}_\perp)\chi_{(2\to 2)}(y,\mathbf{l}_\perp)$, which in general depends on x and $\mathbf{k}_\perp$. The reliability of this constant approximation was checked by examining the frame-independence of our numerical results using the sum rule given by Eq. (30), i.e. the exact results of $\mathcal{F}_\pi(\xi,x,t)$ and $F_\pi(t)$ obtained from the true values of G_π given by Fig. 6 were compared with those obtained from our single averge value of $G_\pi = 0.32$ for all (ξ,t). The numerical results of our constant G_π prescription have shown definite improvement (better than 90 % accuracy for $\xi \lesssim 0.9$) to restore the frame-independence of our model (see Figs. 7- 9) and seemed to be a quite reliable approximation. Our model also satisfies the polynomiality conditions for $n = 2$ and 3 moments of the SQDs (See Fig. 10) and our value of F_3^v is in good agreement with the QCD sum-rule result with non-local condensates [25]. Moreover, the ordinary quark distribution amplitude of the pion ($\phi_\pi(y = 2x-1)$) can be obtained from the two-pion distribution amplitude in $\xi = 0$ and $t = 0$ limit where one of the produced pions becomes soft. Our result of ϕ_π is very close to the asymptotic quark distribution amplitude consistent with the CLEO measurements [29]. The isosinglet skewed quark distribution amplitude in the pion (See Fig. 11) is also consistent with the result satisfying the low-energy soft pion theorem [5].

For the model improvement, however, it would be necessary to consider not only the dynamical quark mass discussed in our previous work [14] but also the B-S amplitude for the quark-gauge boson vertex to remove the apparent discontinuity at $x = \xi$ as shown in Figs.7 and 8. Especially, in exploring the new physics associated with the SQDs for the treatment of the pion form factor, we note from Eq. (9) that the definition of $\mathcal{F}_\pi$ involves the matrix element of the light-front operator present in the three-point approach to quark distributions of hadrons in scaling regions. As was shown in Ref. [30] the treatment of such operators can lead one to consider nonlocal quark condensates, which can introduce nonperturbative QCD structure in the quark-gauge boson vertex. This will be a subject of future research by the authors.

Acknowledgements

The work of HMC and LSK was supported in part by the NSF grant PHY-00070888 and that of CRJ by the US DOE under grant No. DE-FG02-96ER40947. The North Carolina Supercomputing Center and the National Energy Research Scientific Computer Center are also acknowledged for the grant of Cray time.

[1] Müller, D. Robaschik, B. Geyer, F. M. Dittes, J. Hořejši, Fortsch. Phys. **42**, 101 (1994) [hep-ph/9812448].
[2] X. Ji, Phys. Rev. Lett. **78**, 610 (1997); Phys. Rev. D **55**, 7114 (1997).
[3] A. V. Radyushkin, Phys. Rev. D **56**, 5524 (1997).
[4] J. C. Collins, L. Frankfurt, and M. Strikman, Phys. Rev. D **56**, 2982 (1997).
[5] M. V. Polyakov and C. Weiss, Phys. Rev. D **60**, 114017 (1999).
[6] J. Blümlein, B. Geyer, D. Robaschik, Nucl. Phys. B **560**, 283 (1999);
J. Blümlein and D. Robaschik, Nucl. Phys. B **581**, 449 (2000).
[7] M. Diehl, Th. Feldmann, R. Jakob, and P. Kroll, Eur. Phys. J. **C**, 409 (1999).
[8] S.-J. Brodsky, M. Diehl, and D. S. Hwang, Nucl. Phys. B **596**, 99 (2001).
[9] M. Burkardt, Phys. Rev. D **62**, 094003 (2000).
[10] M. Diehl, Th. Feldmann, R. Jakob, and P. Kroll, Nucl. Phys. B **596**, 33 (2001).
[11] W. Jaus, Phys. Rev. D **44**, 2851 (1991).
[12] H. -M. Choi and C. -R. Ji, Phys. Rev. D **59**, 074015 (1999).
[13] H. -M. Choi and C. -R. Ji, Phys. Rev. D **56**, 6010 (1997).
[14] L. S. Kisslinger, H.-M. Choi, and C.-R. Ji, Phys. Rev. D **63**, 113005 (2001).
[15] S. J. Brodsky and D. S. Hwang, Nucl. Phys. B **543**, 239 (1998).
[16] C.-R. Ji and H.-M. Choi, to be published in Phys. Lett. B [hep-ph/0009281].
[17] S. J. Brodsky, C.-R. Ji and M. Sawicki, Phys. Rev. D **32**, 1530 (1985).
[18] J. H. O. Sales, T. Frederico, B. V. Carlson, and P. U. Sauer, Phys. Rev. C **61**, 044003 (2000).
[19] M. B. Einhorn, Phys. Rev. D **14**, 3451 (1976).
[20] X. Ji, W. Melnitchouk, and X. Song, Phys. Rev. D **56**, 5511 (1997).
[21] A. V. Radyushkin, Phys. Lett. B **449**, 81 (1999).
[22] R. A. Amendolia et al., Phys. Lett. B **178**, 435 (1985).
[23] J. Volmer et al., Phys. Rev. Lett. **86**, 1713 (2001).
[24] V. Yu. Petrov et al., Phys. Rev. D **57**, 4325 (1998).
[25] A. V. Belitsky, Phys. Lett. B **386**, 359 (1996).
[26] V. L. Chernyak and I. R. Zhitnitsky, Phys. Rep. **112**, 1783 (1984).
[27] S. V. Mikhailov and A. V. Radyushkin, Phys. Rev. D **45**, 1754 (1992).
[28] C.-R. Ji, P. L. Chung, and S. R. Cotanch, Phys. Rev. D **45**, 4214 (1992).
[29] CLEO Collaboration, J.Gronberg *et al.*, Phys. Rev. D **57**, 33 (1998).
[30] H. Jung and L.S Kisslinger, Nucl. Phys. A **586**, 682 (1995).

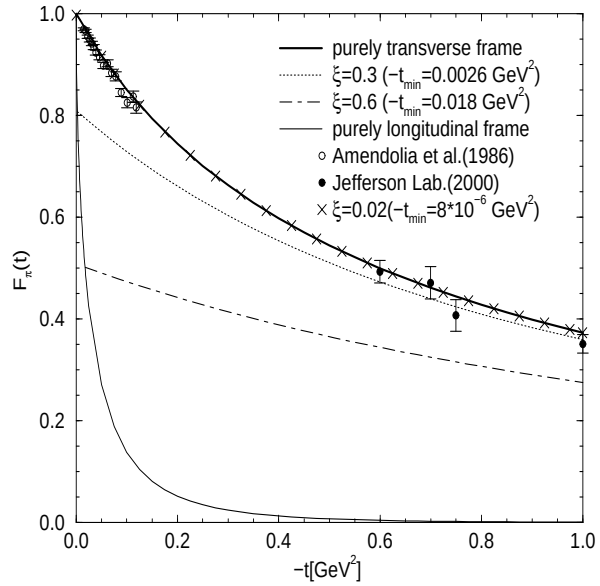

FIG. 5. The valence contribution to the pion EM form factor with different skewedness parameters ξ compared with the experimental data [22,23].

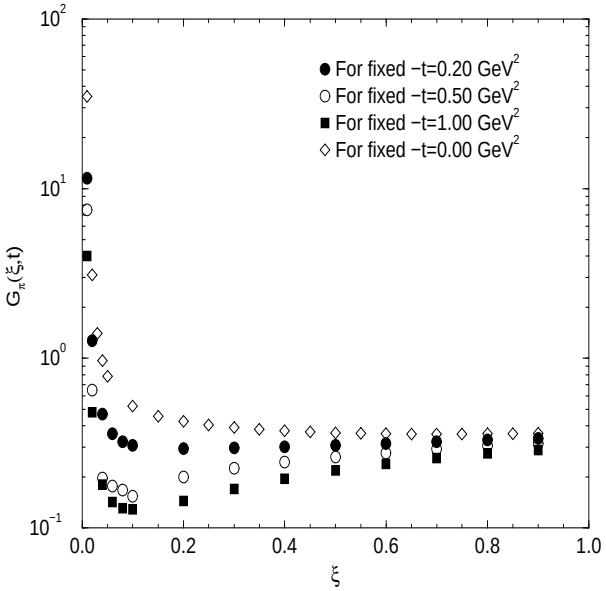

FIG. 6. The ξ-dependence of G_π for different momentum transfers $-t = 0$ (diamond), 0.2 (black circle), 0.5(white circle), and 1 (black square) [GeV^2], respectively.

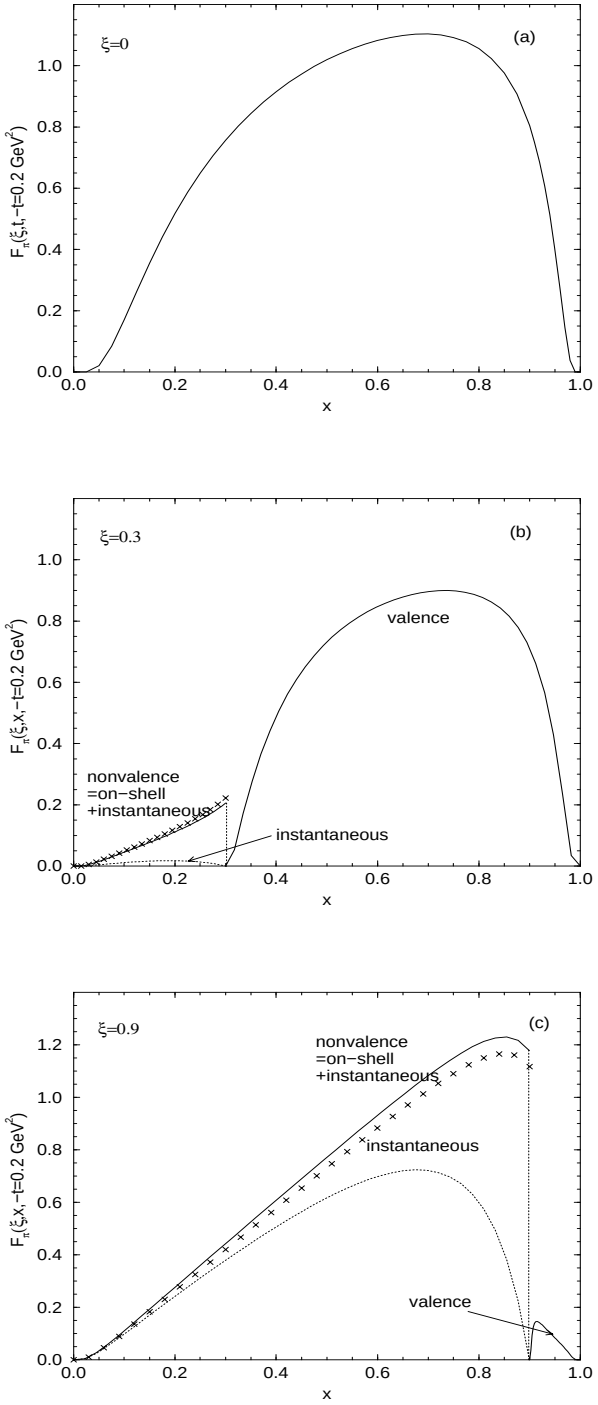

FIG. 7. Skewed quark distributions of the pion at $-t = 0.2$ GeV^2 with $\xi = 0$ in (a) ,0.3 in (b), and 0.9 in (c), respectively. The solid [cross (x)] line in nonvalence contribution represents the full result of using true [average] G_π value and the dotted line represents the instantaneous part of the nonvalence contribution.

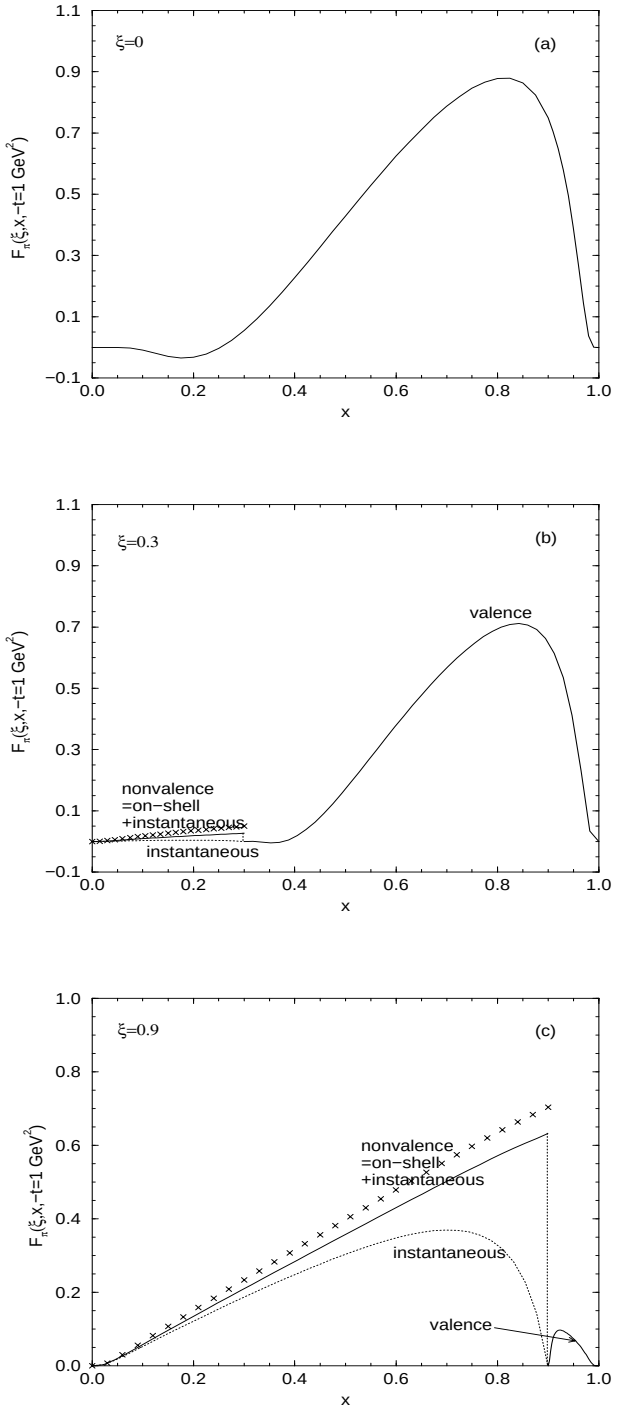

FIG. 8. Skewed quark distributions of the pion at $-t = 1$ GeV^2 with different $\xi = 0$ in (a), 0.3 in (b), and 0.9 in (c), respectively. The same line code is used as in Fig. 7.

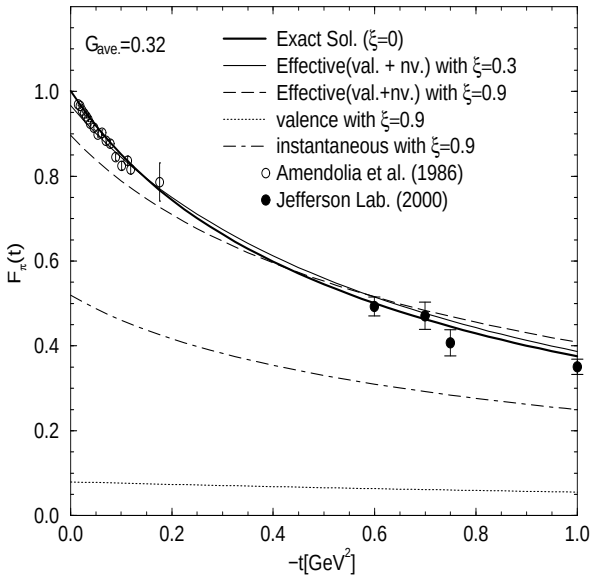

FIG. 9. The effective solution of pion form factor using a common average $G_\pi = G_{\rm ave.} = 0.32$ value for $\xi = 0.3$ (thin solid line) 0.9 (long-dashed line) compared with the exact solution (thick solid line) as well as experimental data [22,23]. The dotted and dot-dashed lines represent the valence and instantaneous contributions to the form factor for $\xi = 0.9$ case, respectively.

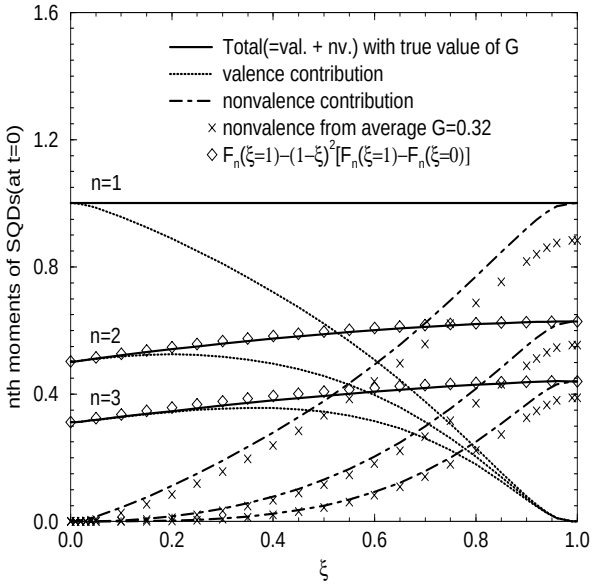

FIG. 10. The nth moments $F_n(\xi, -t)$ of SQDs of the pion at $t = 0$ using the true value of G. The total results(thick solid lines) for $n = 2$ and 3 are well fitted by the simple polynomial(diamond) in ξ. For comparison, we include the nonvalence contributions obtained from the average $G_\pi = 0.32$(cross lines).

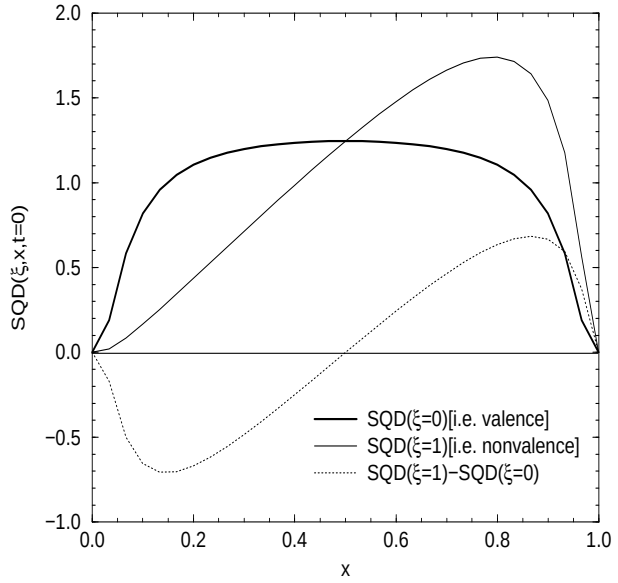

FIG. 11. The SQDs of the pion at $t = 0$ using the true value of G(=0.384). The thick solid, solid, and dotted lines represent $\mathcal{F}_\pi(\xi = 0, x, t = 0)$(valence), $\mathcal{F}_\pi(\xi = 1, x, t = 0)$(nonvalence), and their difference $\mathcal{F}_\pi(\xi = 1, x, t = 0) - \mathcal{F}_\pi(\xi = 0, x, t = 0)$, respectively.

TABLE I. The nth moments $F_n(\xi, x, t = 0)$ of the SQDs for the pion where $F_n^v = F_n(\xi = 0)$ and $F_n^{nv} = F_n(\xi = 1)$ represent pure valence and pure nonvalence contributions, respectively.

Model	$F_2^v[F_2^{nv}]$	$F_3^v[F_3^{nv}]$	$F_4^v[F_4^{nv}]$	$F_5^v[F_5^{nv}]$	$F_6^v[F_6^{nv}]$	$F_7^v[F_7^{nv}]$
Ours	0.503[0.623]	0.312[0.433]	0.215[0.322]	0.16[0.25]	0.123[0.201]	0.098[0.165]
[5]		0.25[–]				
[25]		0.29[–]				

TABLE II. The nth moments $\langle y_n \rangle$ of the ordinary quark distribution amplitude $\phi_\pi(y)$ for the pion.

Model	$\langle y_1 \rangle$	$\langle y_2 \rangle$	$\langle y_3 \rangle$	$\langle y_4 \rangle$	$\langle y_5 \rangle$	$\langle y_6 \rangle$
Ours	0.0	0.239	0.0	0.109	0.0	0.062
[26]	0.0	0.43	0.0	0.24	0.0	0.15
[27]	0.0	0.25	0.0	0.12	0.0	0.07
[28][c]	0.0	0.25	0.0	0.11	0.0	0.06

[a] For the gaussian parameter $\beta = 0.36$ GeV in Ref. [28].